# Thermally Stable Nanocrystalline TiO2 Photocatalysts Synthesized via Sol−Gel Methods Modified with Ionic Liquid and Surfactant Molecules

**4 AUTHORS**, INCLUDING:

Rajender S Varma

United States Environmental Protection Age…

**540** PUBLICATIONS **15,430** CITATIONS

SEE PROFILE

Dionysios D Dionysiou

University of Cincinnati

**339** PUBLICATIONS **9,962** CITATIONS

SEE PROFILE

# Thermally Stable Nanocrystalline TiO₂ Photocatalysts Synthesized via Sol−Gel Methods Modified with Ionic Liquid and Surfactant Molecules

Hyeok Choi,[†] Yong Jin Kim,[‡,§] Rajender S. Varma,[‡] and Dionysios D. Dionysiou*,[†]

*Department of Civil and Environmental Engineering, University of Cincinnati, Cincinnati, Ohio 45221-0071, and Clean Processes Branch, National Risk Management Research Laboratory, U.S. Environmental Protection Agency, Cincinnati, Ohio 45268*

*Received July 6, 2006. Revised Manuscript Received August 13, 2006*

Recently, sol−gel methods employing ionic liquids (ILs) have shown significant implications for the synthesis of well-defined nanostructured inorganic materials. Herein, we synthesized nanocrystalline TiO₂ particles via an alkoxide sol−gel method employing a water-immiscible room temperature IL (1-butyl-3-methylimidazolium hexafluorophosphate, [bmim][PF₆]) as a new solvent medium and further modified with nonionic surfactant (polyoxyethylenesorbitan monooleate) as a pore templating material. Detailed information on the preparative method, synthesis route and mechanism, crystallographic and structural properties, and photocatalytic activity of the TiO₂ particles is described. The possible rationale for the formation of nanocrystalline TiO₂ particles with high surface area and activity is discussed with respect to the special characteristics of [bmim][PF₆] as well as the role of the surfactant self-assembly in the sol−gel network. Due to its capping effect and water immiscibility, the use of [bmim][PF₆] in sol−gel synthesis of TiO₂ induces controlled hydrolysis of titanium alkoxide precursor, resulting in a stable sol−gel network with an ordered array, and localized water-poor conditions, resulting in the formation of completely condensed and directly crystalline systems at ambient condition. The low surface energy and adaptability of [bmim][PF₆] facilitate the generation of very small nanocrystalline TiO₂ particles and then it also acts as a particles aggregation inhibitor. The ensuing TiO₂ particles have good thermal stability to resist pore collapse and anatase-to-rutile crystal phase transformation during thermal treatment.

## Introduction

Due to its high reaction rates and short treatment times to decompose recalcitrant organic chemicals in water, TiO₂-based advanced oxidation technology has been extensively researched in environmental remediation.[1−8] To enhance the activity and widespread application of TiO₂ photocatalyst for water and air treatment, several previous studies have focused on the control of the physicochemical properties of TiO₂, (i.e., grain size, morphology, and crystal phase) and especially on the synthesis of nanostructured TiO₂ because of its attractive optical, electrical, chemical, and catalytic properties.[9−11] Fabrication of well-defined nanostructured TiO₂ or other inorganic oxides has been achieved via sol−gel methods modified with self-assembly of amphiphilic organic molecules (i.e., surfactants, block copolymers) as pore-forming agents in the inorganic network.[2,7,8,12−16] The sol−gel method is one of the most convenient processes for the preparation of TiO₂ due to its ability to tailor-design the structural properties of TiO₂ with mesoporous inorganic matrix as well as its versatile applications in fabricating TiO₂ thin films and membranes over other synthesis methods such as flame synthesis, hydrolysis precipitation, and hydrothermal synthesis.[2,6−8,16,17]

In conventional solvents used in sol−gel synthesis of TiO₂, the hydrolysis and condensation reactions of titanium alkoxide precursors are too fast, resulting in uncontrolled physicochemical properties of TiO₂.[16] The synthesis method, regardless of hydrolytic or non-hydrolytic reaction pathways, typically yields amorphous TiO₂, which needs further heat treatment for crystallization.[17] However, the TiO₂ inorganic network, like some other non-silica oxides, is not thermally stable enough to resist breakage of the initial nanostructured Ti−O−Ti inorganic matrix and anatase-to-rutile crystal phase transformation during thermal treatment.[18] The last two are more critical in case of employing pore templating strategies. As a result, it is beneficial to synthesize nanocrystalline TiO₂

* To whom correspondence should be addressed. E-mail: dionysios.d.dionysiou@uc.edu. Phone: 513-556-0724. Fax: 513-556-2599.
† University of Cincinnati.
‡ U.S. Environmental Protection Agency.
§ Current address: Environment and Energy Division, Korea Institute of Industrial Technology, Chonan-si, 330-825, South Korea.

(1) Fujishima, A.; Honda, K. *Nature* **1972**, *238*, 37.
(2) Choi, H.; Stathatos, E.; Dionysiou, D. D. *Appl. Catal. B* **2006**, *63*, 60.
(3) Ollis, F. D., Al-Ekabi, H., Eds. *Photocatalytic Purification and Treatment of Water and Air*; Elsevier Science: Amsterdam, 1993.
(4) Hoffmann, M. R.; Martin, S. T.; Choi, W.; Bahnemann, D. W. *Chem. Rev.* **1995**, *95*, 69.
(5) Fujishima, A., Hashimoto, K., Watanabe, T., Eds. *TiO₂ Photocatalysis: Fundamentals and Applications*; BKC Inc.: Tokyo, 1999.
(6) Dionysiou, D. D.; Burbano, A. A.; Suidan, M. T.; Baudin, I.; Laîné, J. M. *Environ. Sci. Technol.* **2002**, *36*, 3834.
(7) Choi, H.; Sofranko, A. C.; Dionysiou, D. D. *Adv. Funct. Mater.* **2006**, *16*, 1067.
(8) Choi, H.; Stathatos, E.; Dionysiou, D. D. *Thin. Solid Films* **2006**, *510*, 107.
(9) Fox, M. A.; Dulay, M. T. *Chem. Rev.* **1993**, *93*, 54.
(10) Fotou, G. P.; Pratsinis, S. *Chem. Eng. Commun.* **1996**, *151*, 251.
(11) Caruso, F. *Adv. Mater.* **2001**, *13*, 11.

(12) Antonelli, M.; Ying, J. Y. *Angew. Chem., Int. Ed. Engl.* **1995**, *34*, 2014.
(13) Yang, P.; Zhao, D.; Margolese, D. I.; Chmelka, B. F.; Stucky, G. D. *Chem. Mater.* **1999**, *11*, 2813.
(14) Peng, Z.; Shi, Z.; Liu, M. *Chem. Commun.* **2000**, 2125.
(15) Yoshitake, H.; Sugihara, T.; Tatsumi, T. *Chem. Mater.* **2002**, *14*, 1023.
(16) Brinker, J., Scherer, G. W., Eds. *Sol−Gel Science: The Physics and Chemistry of Sol−Gel Processing*; Academic Press: San Diego, 1990.
(17) Zhou, Y.; Antonietti, M. *J. Am. Chem. Soc.* **2003**, *125*, 14960.

particles with high surface area and activity at ambient condition (e.g., room temperature), allowing for a wider selection of support materials to be coated as well as avoiding heat treatment at high temperature.

Recently, alkoxide sol−gel methods employing ionic liquids (ILs) have been introduced for the synthesis of inorganic materials with unique shape and structure since ILs possess tunable solvent properties so that they can easily interact with various surface and chemical reaction environments.[17,19−28] In particular, room temperature ILs (RTILs), which are usually composed of a large organic cation and a weakly coordinating anion, are of great interest due to their advantageous physical and chemical properties, such as low melting point, negligible vapor pressure, and high thermal stability.[21−28] In addition, RTILs with hydrophobic regions and a high directional polarizability form extended hydrogen bond systems in the liquid state, resulting in a highly structured self-assembly of RTILs without the formation of ordered micelle structure of hydrophilic and hydrophobic chains as in long-chain surfactants.[21,29,30] This organized assembly was reported to be able to act as a template for the preparation of well-defined nanoparticles, nanorods, and other nanostructured inorganic materials.[25−27] In previous studies, nanocrystalline $TiO_2$ particles were also synthesized at ambient conditions via sol−gel methods employing RTILs most probably (i.e., still not clear) due to the self-assembly of RTILs as a pore template.[21,22] However, few studies were focused on understanding the synthesis route and mechanism of $TiO_2$ in this sol−gel method, beyond the role of RTILs as a template, since the growth of $TiO_2$ nanocrystals in RTILs solution at room temperature is a very complex process. In addition, limited experimental information on the effect of RTILs on the physicochemical properties and photocatalytic activity of $TiO_2$ has been reported.

Herein, we synthesized nanocrystalline $TiO_2$ particles via an alkoxide sol−gel method employing water-immiscible RTIL as a solvent medium and later modified with nonionic surfactant as a pore-templating material. Detail information on the preparative method, crystallographic and structural properties, and photocatalytic activity of the $TiO_2$ particles is described. The possible synthesis route and mechanism of the $TiO_2$ particles and advantages of using water-immiscible RTILs in this sol−gel method are discussed in comparison with the challenges of conventional solvent systems.

(18) Bosc, F.; Ayral, A.; Albouy, P.-A.; Datas, L.; Guizard, C. *Chem. Mater.* **2004**, *16*, 2208.
(19) Welton, T. *Chem. Rev.* **1999**, *99*, 2071.
(20) Wasserscheid, P.; Keim, W. *Angew. Chem., Int. Ed. Engl.* **2000**, *39*, 3772.
(21) Zhou, Y.; Schattka, J. H.; Antonietti, M. *Nano Lett.* **2004**, *4*, 477.
(22) Yoo, K.; Choi, H.; Dionysiou, D. D. *Chem. Commun.* **2004**, 2000.
(23) Liu, Y.; Li, J.; Wang, M.; Li, Z.; Liu, H.; He, P.; Yang, X.; Li, J. *Cryst. Growth Des.* **2005**, *5*, 1643.
(24) Zhou, Y. *Curr. Nanosci.* **2005**, *1*, 35.
(25) Jiang, Y.; Zhu, Y.-J. *J. Phys. Chem. B* **2005**, *109*, 4361.
(26) Jiang, J.; Yu, S.-H.; Yao, W.-T.; Ge, H.; Zhang, G. Z. *Chem. Mater.* **2005**, *17*, 6094.
(27) Taubert, A.; Steiner, P.; Mantion, A. *J. Phys. Chem. B* **2005**, *109*, 15542.
(28) Yoo, K.; Choi, H.; Dionysiou, D. D. *Catal. Commun.* **2005**, *6*, 259.
(29) Cammarata, L.; Kazarian, S. G.; Salter, P. A.; Welton, T. *Phys. Chem. Chem. Phys.* **2001**, *3*, 5192.
(30) Antoniou, A.; Kuang, D.; Smarsly, B.; Zhou, Y. *Angew. Chem., Int. Ed.* **2004**, *43*, 4988.

## Experimental Section

**Preparation Procedure.** Titanium tetraisopropoxide (TTIP, Ti-$(OCH(CH_3)_2)_4$, Aldrich) was added to 2-propanol (*i*-PrOH, $(CH_3)_2$-CHOH, Fisher) at an *i*-PrOH/TTIP molar ratio of 30. A water-immiscible RTIL (1-butyl-3-methylimidazolium hexafluorophosphate, [bmim][$PF_6$], Sachem) was then added into the mixture at a [bmim]-[$PF_6$]/TTIP molar ratio of 3 and vigorously stirred for 10 min. When the RTIL-templated titania sol was added into water drop by drop up to a $H_2O$/TTIP molar ratio of 100 at room temperature, hydrolysis and condensation reactions occurred, forming a precipitate of white $TiO_2$ particles. The solution was stirred vigorously for 30 min, and the $TiO_2$ particles were recovered by filtration with a fine filter paper (P2, Fisher), washed thoroughly with water, and dried at 100 °C for 2 h in an oven (model 5015-50, Cole-Parmer). The entrapped [bmim][$PF_6$] and organic residues were removed by extraction with acetonitrile ($C_2H_3N$, Fisher) for 12 h. Then, the $TiO_2$ particles were recovered again by filtration, washed with acetonitrile and water several times, and dried at room temperature for 24 h. The obtained product was a white fine powder. For comparison using a relatively water-miscible RTIL, 1-butyl-3-methylimidazolium tetrafluoroborate ([bmim][$BF_4$], Aldrich) was added into the solution instead of the water-immiscible [bmim]-[$PF_6$]. For abbreviations, $S_{control}$, $S_{PF6}$, and $S_{BF4}$ represent $TiO_2$ particles prepared without RTIL, with [bmim][$PF_6$], and with [bmim][$BF_4$], respectively. For further modification of [bmim][$PF_6$]-templated sol−gel method with surfactant templates, polyoxyethylenesorbitan monooleate (Tween 80, Aldrich) as a nonionic surfactant was dissolved in *i*-PrOH. Then, [bmim][$PF_6$] followed by TTIP was added into the solution. The mixture was added into water. The molar ratio of Tween 80 to TTIP was 1. The corresponding $TiO_2$ particles are denoted as $S_{PF6,T80}$.

The $TiO_2$ particles were subsequently heat-treated at elevated temperatures (up to 1000 °C) to increase materials cyrstallinity and to remove any impurities and surfactant templates using a multi-segment programmable furnace (Paragon model HT-22-D, Thermcraft) in the presence of air. The temperature of the furnace was increased at a ramp rate of 3.0 °C/min to a final temperature and held for 1 h. Then, the furnace was allowed to cool gradually to room temperature.

**Materials Characterization.** A Kristalloflex D500 diffractometer (Siemens) with Cu Kα ($\lambda = 1.5406$ Å) radiation was used for X-ray diffraction (XRD) analysis to determine the crystal phase of $TiO_2$. For each scan, $2\theta$ was increased from 20.0 to 60.0 deg with a step of 0.1 and time-to-step ratio of 1.0. Accelerated surface area and porosimetry (ASAP model 2020 and Tristar 3000, Micromeritics) was applied to measure the Brunauer−Emmett−Teller (BET) surface area and adsorption isotherm-based Barrett−Joyner−Halenda (BJH) pore size distribution and pore volume (or porosity) of the materials using nitrogen adsorption and desorption isotherms. Before the measurement, the samples were purged with helium gas for 2 h at 150 °C or 12 h at 40 °C using Flow Prep 060 (Micromeritics). The morphology of $TiO_2$ particles was examined using a JEM-2010F (JEOL) high-resolution transmission electron microscope (HR-TEM) at 200 kV after dispersing the samples in methanol using an ultrasonicator (2510R-DH, Bransonic) for 5 min followed by their fixation on a carbon-coated copper grid (LC200-Cu, EMS). Compositional analysis of $TiO_2$ was conducted using an energy-dispersive X-ray spectroscope (EDX, Oxford Isis). Particle size of $TiO_2$ was measured using a Zetasizer 3000 HS$_A$ (Malvern Instruments) after $TiO_2$ particles were dispersed in 1.0 mM NaCl solution using a sonicator for 30 min. For the measurement of weight changes and heat flow of $TiO_2$ during heat treatment, thermogravimetric analysis and differential scanning calorimetry (TGA/DSC, SDT 2960, TA instruments) were employed at the same

condition as the heat treatment program used for the synthesis of TiO₂.

**NMR and FTIR Analyses.** To investigate the synthesis route of TiO₂ using the sol−gel method modified with [bmim][PF₆], changes in chemical structure and bonding during the synthesis were tracked with nuclear magnetic resonance (NMR, Bruker AMX300) and Fourier transform infrared (FTIR, Nicolet Magna-IR 760) spectroscopy. For ¹H NMR analysis, approximately 0.1 mL of sample was transferred to the NMR holder containing 1.9 mL of deuterated chloroform (CDCl₃, Aldrich). Along with the NMR analysis, drops of the samples were put onto a potassium bromide (KBr, Sigma) thin pellet for FTIR analysis and scanned 64 times at a resolution of 4 cm⁻¹ in transmission mode with a KBr background. To study the C−H stretching vibrational infrared spectra of the [bmim][PF₆] around 2900 cm⁻¹ and other residual organics, the prepared TiO₂ particles were thoroughly ground, mixed with KBr powder at a ratio of sample:KBr = 1:9, shaped into a 0.1 mm thin pellet, and analyzed.

**Measurement of Photocatalytic Activity.** The photocatalytic activity of TiO₂ particles was measured in terms of 4-chlorophenol (4-CP, Aldrich) degradation. After dispersing the TiO₂ particles in water by sonication (model B-22-4, Branson Ultrasonic Cleaner) for 1 h, the suspension was added into a cylindrical borosilicate reactor with inner diameter of 5.5 cm and recirculated continuously using a pump. Pretreated air passing through an activated carbon column and a humidifier was supplied into an additional flask. The following conditions were kept constant: initial volume of reaction solution = 0.6 L, solution recirculation rate = 0.3 L/min, air flow rate = 0.5 L/min, solution temperature = 25 ± 3 °C, pH = 7.0 ± 0.1 in 10 mM phosphate buffer, initial concentration of 4-CP = 50 mg/L, and TiO₂ dosage = 500 mg/L. Four 15 W low-pressure mercury UV tubes (Spectronics) emitting near UV radiation (300−400 nm) with a peak at 365 nm were used at a light intensity of 1.3 mW/cm² at the center of the reactor. The concentration of 4-CP was determined using a high-performance liquid chromatography (HPLC; series 1100, Agilent) equipped with a C-16 Discovery column (Supelco). The mobile phase was a mixture of acetonitrile and 0.01 N sulfuric acid at a ratio of 30:70 (v/v) with a flow rate of 1.5 mL/min. All chemicals were used as received. The water used in all experiments was double-distilled water (Corning-Mega Pure).

## Results and Discussion

**Physicochemical Properties and Activity of [bmim]-[PF₆]-Templated TiO₂.** As reported previously,[22] despite the low heat treatment temperature of 100 °C, the TiO₂ particles (S_PF6) prepared with [bmim][PF₆] have an anatase crystalline phase with crystallinity of approximately 37%, calculated from the mass fraction of crystals in their XRD pattern.[31] The crystal size was around 5 nm. Compared to previously reported results,[32,33] the pore size distribution of the S_PF6 was narrow, ranging only from 2.0 to 7.5 nm. The BET surface area and pore volume of the material were 273 ± 7.4 m²/g and 0.296 ± 0.011 cm³/g, respectively. The HR-TEM image in Figure 1a clearly shows the morphology of anatase-containing nanostructured S_PF6 (note Supporting Information Figure S1 for the HR-TEM images of S_BF4, where many tiny

(31) Young, R. J. *Introduction to Polymers*; Chapman and Hall: New York, 1981.
(32) Sing, K. S. W.; Everett, D. H.; Haul, R. A. W.; Moscow, L.; Pierotti, R. A.; Rouquerol, J.; Siemieniewska, T. *Pure Appl. Chem.* **1985**, *57*, 603.
(33) Wang, L.; Tomura, S.; Maeda, M.; Ohashi, F.; Inukai, K.; Suzuki, M. *Chem. Lett.* **2000**, *29*, 1414.
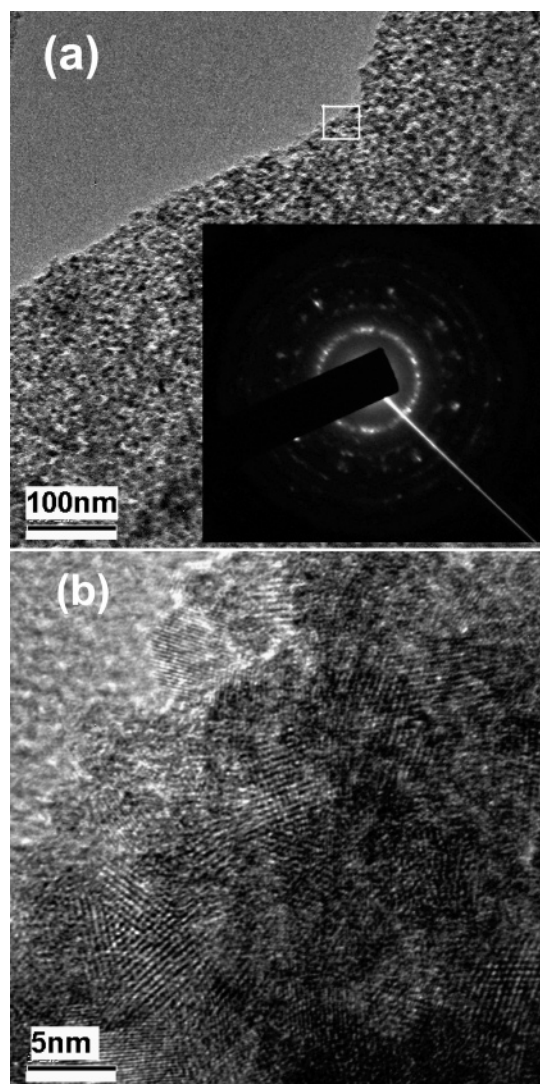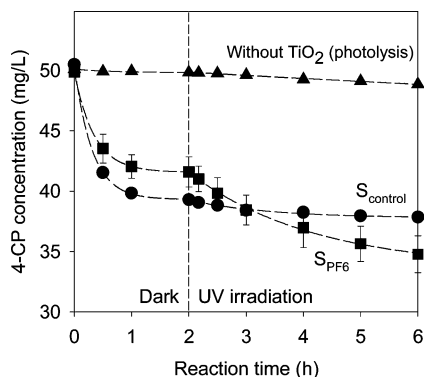
**Figure 1.** HR-TEM images of [bmim][PF₆]-templated TiO₂ (S_PF6) calcined at 100 °C. Inset is a selected area electron diffraction pattern.

pores with size of 2−3 nm are observed but the density of the pores is low, resulting in low specific surface area of 141 m²/g and pore volume of 0.046 cm³/g as compared to those of S_PF6). It is observed that S_PF6 was almost exclusively composed of small sized nanocrystallites. The S_PF6 was highly porous, and all areas of the samples showed more or less similar pore morphology, a disordered mesostructure without long-range order in the pore arrangement. The micrograph in Figure 1b shows several randomly oriented nanocrystallites, ranging in size from 4.5 to 6.0 nm with sets of clearly resolved lattice fringes thereby indicating that the S_PF6 is highly crystalline. The crystallinity of S_PF6 was additionally confirmed by the selected area electron diffraction pattern inserted in Figure 1a, revealing diffraction rings typical for a crystalline powder due to the absence of an amorphous halo.

Figure 2 shows 4-CP adsorption and degradation by S_control and S_PF6 prepared at 100 °C. Due to its high surface area of 473 m²/g, S_control had a higher adsorption capacity. After 2 h in the dark, 4-CP adsorption on TiO₂ particles reached a pseudo-steady state. As expected from the crystallographic analysis of S_control and S_PF6, the anatase crystal phase-containing S_PF6 had a photocatalytic activity as compared to

**Figure 2.** 4-CP adsorption and photocatalytic degradation by control TiO$_2$ (S$_{control}$) and [bmim][PF$_6$]-templated TiO$_2$ (S$_{PF6}$) calcined at 100 °C. Error bars indicate the standard deviation of triplicated results.

the amorphous S$_{control}$. It is well-known that no considerable photocatalytic activity is observed for the amorphous TiO$_2$ due to large numbers of bulk defects where the photogenerated electrons and holes are recombined simultaneously. Although the activity is relatively low, the low synthesis temperature is an advantage in the synthesis method.

**Synthesis Route and Mechanism of [bmim][PF$_6$]-Templated TiO$_2$.** The synthesis process for the highly porous crystalline TiO$_2$ particles in this study is depicted in Scheme 1. To better understand the formation of the TiO$_2$ sol−gel network, a series of NMR/FTIR studies were carried out. The formation of TiO$_2$ sol in preparation step I shown in Scheme 1 was evidenced from a mixture of [bmim][PF$_6$] and TTIP in CDCl$_3$. As shown in Figure 3 along with resonance peaks for [bmim][PF$_6$] marked as 1−6, TTIP as 7 and 8, and CDCl$_3$ as 11, the concomitant generation of new resonance peaks marked as 9 and 10, which correspond to free *i*-PrOH, was observed. The in-situ formation of *i*-PrOH is because of the reaction of isopropyl groups in TTIP with hydroxyl groups in [bmim][PF$_6$] containing a small quantity of water up to 0.26−0.42%.[29,34] No direct chemical bonding between [bmim][PF$_6$] and TTIP was observed. After stabilizing the [bmim][PF$_6$]/TTIP mixture for 12 h, an obvious phase separation was observed due to the water immiscibility of [bmim][PF$_6$]. FTIR analysis shown in Figure 4 verified the Ti−O bond formation. The upper layer was composed of TTIP, and the broad band in 3500−3200 cm$^{-1}$ indicated bonded hydroxyl groups of the newly formed *i*-PrOH. On the other hand, the bottom layer was found to be [bmim][PF$_6$], and new peaks at around 824 cm$^{-1}$ can be assigned to the characteristic Ti−O−Ti stretching frequency. These results suggest that the small quantity of water in the [bmim][PF$_6$] would initiate the formation of Ti−O−Ti bond and the TiO$_2$ particles would be homogeneously dispersed only in the hydrophobic [bmim][PF$_6$] phase. However, the role of water in the [bmim][PF$_6$] is complex, and its structure and chemical reactivity seem to be different from those of bulk water as it is tightly bound and activated in the hydrogen bond system of the [bmim][PF$_6$].[29,35,36]

In preparation step II shown in Scheme 1, where the nonreacted TTIP is completely hydrolyzed, the [bmim][PF$_6$] acts

as a capping agent for preventing direct hydrolysis of TTIP due to its water immiscibility. The reduced hydrolysis rate makes it possible to achieve a longer aging time for the formation of a stable sol−gel network possibly with an ordered array. The stability of TiO$_2$ sol−gel network was further verified during heat treatment (see the next section). The capping effect of [bmim][PF$_6$] also makes a localized anhydrous or water-poor area between [bmim][PF$_6$] and inorganic starting material, TTIP. It is usually observed that this water-poor condition can suppress the formation of hydroxide and oxyhydrate and generation of amorphous species as limited amounts of water drive the mass balance to completely condensed and directly crystalline systems.[17] Also, in conventional sol−gel solvent systems employing excessive amount of water (surface tension, $\gamma = 72$ mJ/m$^2$ at 293 K), the nucleation of TiO$_2$ is slow while low interface energy ($\gamma = 46$ mJ/m$^2$ at 293 K) and adaptability of the [bmim][PF$_6$] result in high nucleation rates, generating very small nanocrystalline particles.[17,30,37] Homogeneity of TiO$_2$ nanoparticles dispersed in sol−gel network was retained throughout the entire aging process, and no phase separation was observed. In a previous study, a reaction-limited aggregation theory where a small portion of particle collisions results in limited adherence of particles in the presence of IL was proposed to explain the formation of these highly porous nanocrystals.[17] To verify how the presence of [bmim][PF$_6$] initially affected the particle adherence, particle size of agglomerated TiO$_2$ was measured when the [bmim][PF$_6$]/TTIP mixture in *i*-PrOH was added into water, as shown in Figure 5. In the absence of any RTILs or in the presence of [bmim]-[BF$_4$], large TiO$_2$ clusters were formed in average size of 856 and 690 nm, respectively. However, the presence of [bmim][PF$_6$] significantly reduced the cluster size to 291 nm, resulting from inhibition of TiO$_2$ particle aggregation. These results imply that the water immiscibility of [bmim][PF$_6$] successfully controlled the hydrolysis reaction of TTIP and thus made it possible to homogeneously disperse the particles in the [bmim][PF$_6$] phase, resulting in the formation of highly porous TiO$_2$ particles. In addition, a highly structured frame from the extended hydrogen bond system in [bmim][PF$_6$] is well-known to act as a template for the well-defined nanostructured particles.[21,29,38] The [bmim][PF$_6$] template was just entrapped in the growing covalent titania network rather than being chemically bound to the inorganic matrix, which was evidenced by the NMR and FTIR analyses. Since the [bmim]-[PF$_6$] does not form any chemical bonds with TiO$_2$, the [bmim][PF$_6$] can be easily removed through extraction.[17,39]

In preparation step III shown in Scheme 1, where solvents and [bmim][PF$_6$] were removed, the [bmim][PF$_6$] provides an attractive method for achieving longer aging time without

(34) Rogers, R. D., Seddon, K. R., Eds. *Ionic Liquids as Green Solvents: Progress and Prospects*; American Chemical Society: Washington, DC, 2003.

(35) Mukhopadhyay, I.; Freyland, W. *Langmuir* **2003**, *19*, 1951.

(36) Elaiwi, A.; Hitchcock, S. B.; Seddon, K. R.; Srinivasan, N.; Tan, Y. M.; Welton, T.; Zora, Z. A. *J. Chem. Soc. Dalton Trans.* **1995**, *21*, 3467.

(37) Law, G.; Watson, P. R. *Langmuir* **2001**, *17*, 6138.

(38) Saha, S.; Hayashi, S.; Kobayashi, A.; Hamaguchi, H. *Chem. Lett.* **2003**, *32*, 740.

(39) Adams, H.; Jimenez Blanco, J.-L.; Chessari, G.; Hunter, C. A.; Low, C. M. R.; Sanderson, J. M.; Vinter, J. G. *Chem. Eur. J.* **2001**, *7*, 3494.

**Scheme 1. Synthesis Route of Porous Anatase Crystalline TiO₂ Particles (S$_{PF6}$) Using Sol−Gel Method Modified with [bmim][PF₆][a]**
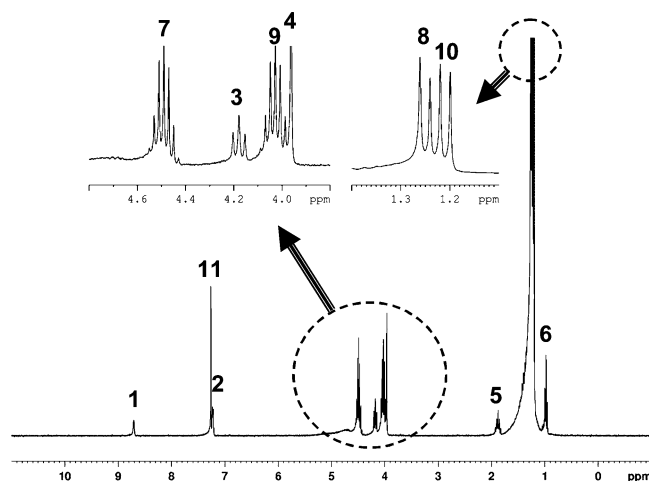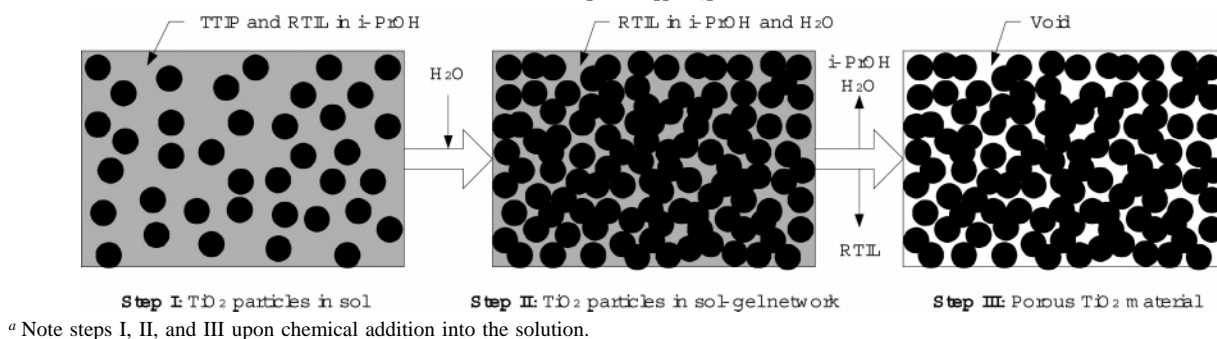


Step I: TiO₂ particles in sol    Step II: TiO₂ particles in sol-gel network    Step III: Porous TiO₂ material

[a] Note steps I, II, and III upon chemical addition into the solution.



**Figure 3.** NMR spectrum of [bmim][PF₆]/TTIP mixture during the synthesis of [bmim][PF₆]-templated TiO₂ (S$_{PF6}$).
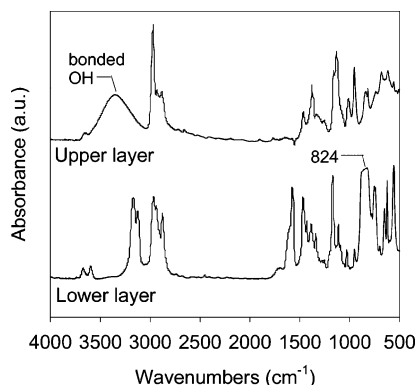


**Figure 4.** FTIR spectra of [bmim][PF₆]/TTIP mixture during the synthesis of [bmim][PF₆]-templated TiO₂ (S$_{PF6}$).

shrinkage of the gel network.[40] Compared to conventional solvents that evaporate quickly before formation of a stable sol−gel network during the aging process, the negligible vapor pressure of the [bmim][PF₆] can prevent gel shrinkage and reduction in surface area.

**Heat Treatment of [bmim][PF₆]-Templated TiO₂.** Table 1 summarizes crystal phase transformation and structural evolution of S$_{control}$ and S$_{PF6}$ upon heat treatment. For S$_{control}$, anatase phase started to appear after heat treatment at 250 °C. The anatase crystallinity of S$_{control}$ calcined at 250−400 °C was comparable to that of S$_{PF6}$ at 100 °C. The anatase phase of S$_{control}$ started to transform to rutile at above 600
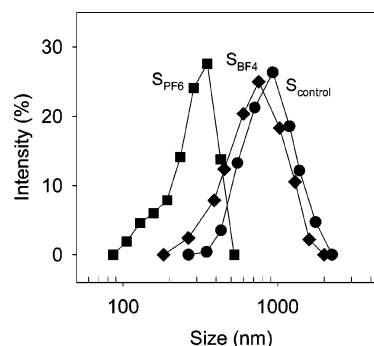


**Figure 5.** Particle size of agglomerated TiO₂ during sol−gel synthesis without IL (S$_{control}$) and with [bmim][PF₆] (S$_{PF6}$) and [bmim][BF₄] (S$_{BF4}$).

°C.[41] On the other hand, S$_{PF6}$ was thermally very stable. Even without further heat treatment, an anatase peak existed. Only the anatase phase was present at up to 900 °C.[42] The thermal stability of S$_{PF6}$ was in good agreement with their structural characteristics. The pore volume and surface area of S$_{control}$ decreased rapidly from 0.707 to 0.046 cm³/g and from 537 to 3.76 m²/g, respectively, while those of S$_{PF6}$ decreased gradually from 0.310 to 0.207 cm³/g and from 282 to 47.9 m²/g upon heat treatment from 20 °C to 800 °C. Consequently, S$_{PF6}$ still kept its highly porous structure, which suppressed solid-state aggregation of the anatase crystallites. The pore size and crystallite size of S$_{PF6}$ even at 800 °C were less than 15 and 20 nm, respectively. On the other hand, the structural properties of S$_{BF4}$ from as-synthesized and calcined at 500 °C were relatively poor as compared to those of S$_{PF6}$ and even those of S$_{control}$ (note Table 2). Although the use of [bmim][BF₄] also affected anatase−rutile crystal phase transformation and thermal stability during calcination, the magnitude of change in such properties was not considerable. The size of as-synthesized and calcined TiO₂ particles was also investigated (Supporting Information Figure S2). As-synthesized S$_{PF6}$ was less aggregated in size of 136 nm as compared to 260 nm for S$_{control}$ and 230 nm for S$_{BF4}$. After heat treatment at 500 °C, size of S$_{control}$ and S$_{BF4}$ significantly increased to 708 and 567 nm, respectively, while S$_{PF6}$ had a more or less small size of 433 nm. These results also support the role of [bmim][PF₆] explained in the section of synthesis route.

(40) Dai, S.; Ju, Y. H.; Gao, H. J.; Lin, J. S.; Pennycook, S. J.; Barnes, C. E. *Chem. Commun.* **2000**, 243.

(41) Gestel, T. V.; Vandecasteele, C.; Buekenhoudt, A.; Dotremont, C.; Luyten, J.; Leysen, R.; der Bruggen, B. V.; Maes, G. *J. Membr. Sci.* **2002**, *207*, 73.

(42) Viswanath, R. N.; Ramasamy, S. *Colloids Surf. A* **1998**, *133*, 49.

**Table 1. Evolution of Crystallographic and Structural Properties of Control TiO$_2$ (S$_{control}$) and [bmim][PF$_6$]-Templated TiO$_2$ (S$_{PF6}$) upon Heat Treatment**

| temp (°C) | crystal phase S$_{control}$ | S$_{PF6}$ | V$_{pore}$ (cm$^3$/g)$^a$ S$_{control}$ | S$_{PF6}$ | S$_{BET}$ (m$^2$/g)$^a$ S$_{control}$ | S$_{PF6}$ | D$_{BJH}$ (nm)$^a$ S$_{control}$ | S$_{PF6}$ | CS$_{XRD}$ (nm)$^a$ S$_{control}$ | S$_{PF6}$ |
|---|---|---|---|---|---|---|---|---|---|---|
| 20 | | anatase | 0.71 | 0.31 | 537 | 282 | 5.4 | 4.2 | | 5.0 |
| 100 | | anatase | 0.68 | 0.30 | 473 | 273 | 5.4 | 5.0 | | 5.1 |
| 250 | anatase | anatase | 0.51 | 0.28 | 315 | 192 | 5.8 | 5.9 | 5.3 | 6.0 |
| 400 | anatase | anatase | 0.39 | 0.27 | 129 | 134 | 9.7 | 7.1 | 10.1 | 8.6 |
| 500 | anatase | anatase | 0.30 | 0.27 | 70.5 | 95.6 | 14.1 | 9.8 | 15.1 | 12.1 |
| 600 | anatase | anatase | 0.24 | 0.26 | 40.4 | 80.1 | 19.6 | 11.6 | 26.7 | 13.5 |
| 700 | A:R = 2:3$^b$ | anatase | 0.10 | 0.25 | 11.6 | 71.0 | 29.4 | 12.2 | | 15.4 |
| 800 | rutile | anatase | 0.05 | 0.21 | 3.8 | 47.9 | 44.6 | 13.4 | | 19.2 |
| 900 | | anatase | | 0.07 | | 7.0 | | 39.0 | | 40.9 |
| 1000 | | rutile | | 0.06 | | 4.2 | | 53.7 | | |

$^a$ V$_{pore}$, pore volume; S$_{BET}$, BET surface area; D$_{BJH}$, BJH average pore diameter from N$_2$ adsorption isotherm branch; CS$_{XRD}$, crystallite size measured from XRD. $^b$ A:R indicates the ratio of anatase and rutile crystal phases.

**Table 2. Physicochemical Properties of TiO$_2$ Particles Prepared under Various Synthesis Conditions**

| synthesis condition | temp (°C) | crystal phase | V$_{pore}$ (cm$^3$/g) | S$_{BET}$ (m$^2$/g) | D$_{BJH}$ (nm) | CS$_{XRD}$ (nm) |
|---|---|---|---|---|---|---|
| no addition (S$_{control}$) | as-synthesized | amorphous | 0.68 | 473 | 5.4 | - |
| | 500 | anatase | 0.30 | 70.5 | 14.1 | 15.1 |
| [bmim][PF$_6$] (S$_{PF6}$) | as-synthesized | anatase | 0.30 | 273 | 5.0 | 5.1 |
| | 500 | anatase | 0.27 | 95.6 | 9.8 | 12.1 |
| [bmim][BF$_4$] (S$_{BF4}$) | as-synthesized | amorphous | 0.05 | 141 | 2.9 | − |
| | 500 | anatase | 0.21 | 51.1 | 14.1 | 13.9 |
| [bmim][PF$_6$] and T80 (S$_{PF6,T80}$) | as-synthesized | anatase | 0.06 | 58.9 | 3.7 | 4.8 |
| | 500 | anatase | 0.31 ± 0.06 | 215 ± 10 | 4.9 | 6.1 |
| T80$^a$ | as-synthesized | amorphous | 0.01 | 10.9 | 3.5 | − |
| | 500 | anatase | 0.04 | 35.9 | 3.8 | 13.0 |

$^a$ TiO$_2$ particles were prepared with T80 surfactant only in the same methodology, which is not properly designed for the use of the surfactant.
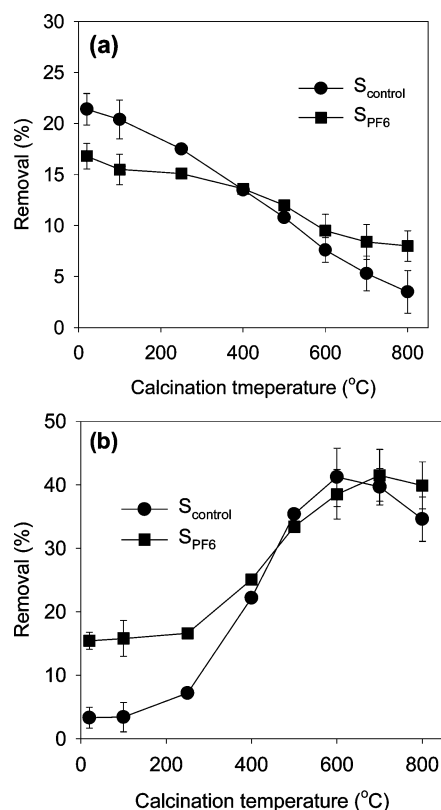


**Figure 6.** (a) 4-CP adsorption and (b) photocatalytic degradation by control TiO$_2$ (S$_{control}$) and [bmim][PF$_6$]-templated TiO$_2$ (S$_{PF6}$).

The physicochemical properties of TiO$_2$ particles were correlated with their adsorption ability and photocatalytic activity, as summarized in Figure 6. The adsorption capacity of the TiO$_2$ particles was a strong function of the surface area upon calcination temperature. It is shown that S$_{PF6}$, even prepared at low temperatures, had considerable photocatalytic activity due to its crystal content and high surface area. Indeed, the photocatalytic activity of S$_{PF6}$ at 100 °C was

comparable to that of S$_{control}$ prepared at 300−400 °C. Moreover, the photocatalytic activity of S$_{PF6}$ with around 37% anatase crystallinity at 100 °C was approximately one-third of that of S$_{PF6}$ at 600−800 °C, where the anatase crystallinity further increased. The photocatalytic activity of S$_{control}$ increased with increasing calcination temperature up to 600 °C, above which the activity decreased due to the reduction in surface area and the anatase−rutile phase transformation.[43] On the other hand, the activity of S$_{PF6}$ was relatively stable, even at up to 800 °C, because of the retention of active anatase phase and the relatively high surface area.[44,45]

**Modification of [bmim][PF$_6$]-Assisted Sol−Gel Method with Surfactant Self-Assembly as Pore Template.** Although many self-assembling strategies have been developed using a variety of surfactants as a templating material to improve the structural and catalytic properties of TiO$_2$ materials, collapse of the initial porous TiO$_2$ inorganic network is accompanied during heat treatment for removing the organic templates and ensuring catalytic activity.[2,18] In this study, the ability of [bmim][PF$_6$] to make TiO$_2$ photocatalysts thermally stable implies that [bmim][PF$_6$]-assisted sol−gel method, once further modified with surfactant templates, can result in the formation of highly porous crystalline TiO$_2$ particles after heat treatment at even high temperatures. To investigate the formation of surfactant self-assembly in [bmim][PF$_6$]-assisted sol−gel method, the assembly size of Tween 80 in *i*-PrOH was measured (Supporting Information Figure S3). The intensity average size of surfactant self-assembly was approximately 3.5 nm. No direct chemical bonding between nonionic Tween 80 and ionic [bmim][PF$_6$] was observed, based on FTIR and NMR

(43) Sclafani, A.; Herrmann, J. M. *J. Phys. Chem.* **1996**, *100*, 13655.
(44) Hsien, Y. H.; Chang, C. F.; Chen Y. H.; Cheng, S. *Appl. Catal. B* **2001**, *31*, 241.
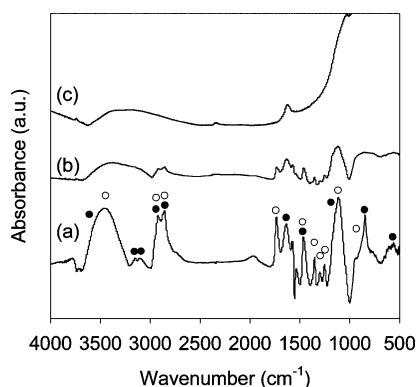(45) Schindler, K. M.; Kunst, M. *J. Phys. Chem. B* **1990**, *94*, 8222.

**Figure 7.** FTIR spectra of TiO₂ (S$_{PF6,T80}$) prepared via [bmim][PF₆]- and surfactant-assisted sol−gel method: (a) as-synthesized before [bmim][PF₆] extraction, (b) as-synthesized, and (c) after heat treatment at 500 °C (●, [bmim][PF₆] peaks; ○, Tween 80 peaks).
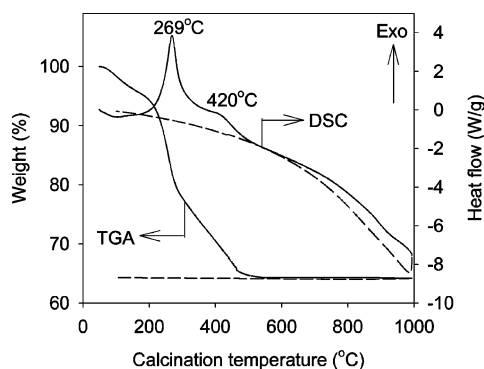


**Figure 8.** TGA/DSC pattern of as-synthesized TiO₂ (S$_{PF6,T80}$) via [bmim]-[PF₆]- and surfactant-assisted sol−gel method.
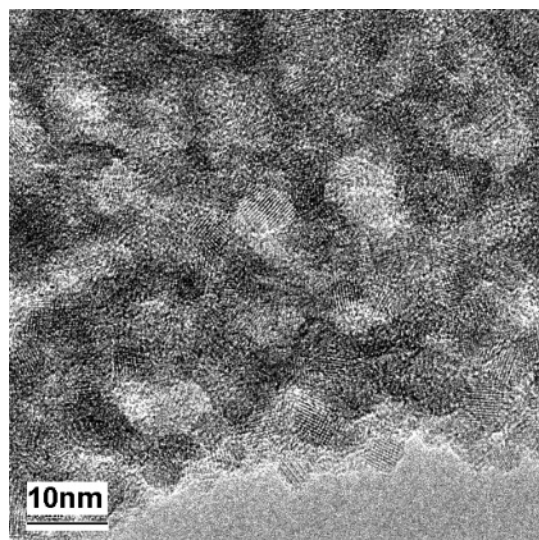


**Figure 9.** HR-TEM morphology of nanostructured anatase crystalline TiO₂ (S$_{PF6,T80}$) prepared via [bmim][PF₆]- and surfactant-assisted sol−gel method at 500 °C.
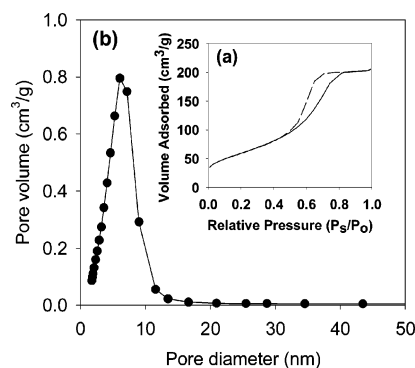


**Figure 10.** (a) N₂ adsorption−desorption isotherms and (b) pore size distribution of TiO₂ (S$_{PF6,T80}$) prepared via [bmim][PF₆]- and surfactant-assisted sol−gel method at 500 °C.

analyses. The surfactant self-assembly is used as a template during hydrolysis and condensation reactions of TTIP and cross-linking of Ti−O−Ti network, resulting in the formation of inorganic−organic nanocomposite.

**Removal of [bmim][PF₆] and Surfactant and Properties of TiO₂.** Before [bmim][PF₆] extraction, S$_{PF6,T80}$ had low surface area of 15.0 m²/g and pore volume of 0.013 cm³/g since [bmim][PF₆] and surfactant added were embedded into the TiO₂ network as shown in Figure 7a. The [bmim][PF₆] was extracted with acetonitrile as shown in Figure 7b where most of [bmim][PF₆] peaks, especially the C−H stretching vibrational IR spectrum of the [bmim][PF₆] around 2900 cm−1, disappeared. Then, S$_{PF6,T80}$ had slightly increased surface area of 58.9 m²/g and pore volume of 0.057 cm³/g. Figure 8 shows result on TGA/DSC analysis for determining a heat treatment temperature required to completely remove all the organic residues embedded in S$_{PF6,T80}$. The as-synthesized S$_{PF6,T80}$ undergoes endothermic desorption of solvents, including water and *i*-PrOH, at low temperature below 120 °C. Exothermic peaks localized at mainly 269 °C and partially 420 °C reflect the processes of oxidation of the organic residuals and anatase crystallization of amorphous structure. Due to the nonionic characteristic of Tween 80, after calcination of S$_{PF6,T80}$ at 500 °C, no significant weight change was observed and the resulting IR spectrum shown in Figure 7c and EDX study of S$_{PF6,T80}$ showed that S$_{PF6,T80}$ was composed of only Ti and O elements.

Figure 9 shows the highly porous inorganic network of S$_{PF6,T80}$ after heat treatment at 500 °C. S$_{PF6,T80}$ has slightly

collapsed spherical bicontinuous structure with highly interconnected network with porosity of 54.8%, indicating that the surfactant used in this synthesis method effectively acted as a pore directing agent. Obvious 5−8 nm pores and many randomly oriented 5−10 nm nanocrystallites with sets of clearly resolved lattice fringes were observed. As shown in Figure 10, the nitrogen adsorption−desorption isotherms of S$_{PF6,T80}$ indicated mesoporous materials. Dissimilar shapes for adsorption and desorption branches implied a different size of pore entrance. The pore size distribution was relatively narrow ranging from 3 to 11 nm, and the BJH pore diameter of 4.91 nm based on adsorption branch was similar to that of the 4.43 nm based desorption branch. The results imply good homogeneity of the pores. Despite the relatively high heat treatment temperature at 500 °C, the BET surface area and pore volume of the material are interestingly high, about 215 m²/g and 0.312 cm³/g, respectively.[18,41] The pore size (3−11 nm from porosimetry and 5−8 nm from TEM image) was significantly larger than the size of the surfactant self-assembly (3.5 nm) due to collapse of the initial pore structure followed by its reorganization during heat treatment.

**Thermal Stability of [bmim][PF₆]- and Surfactant-Templated TiO₂.** The evolution of crystallographic properties of S$_{PF6,T80}$ upon heat treatment was almost similar to that of S$_{PF6}$ described in Table 1 (also note Supporting Informa-
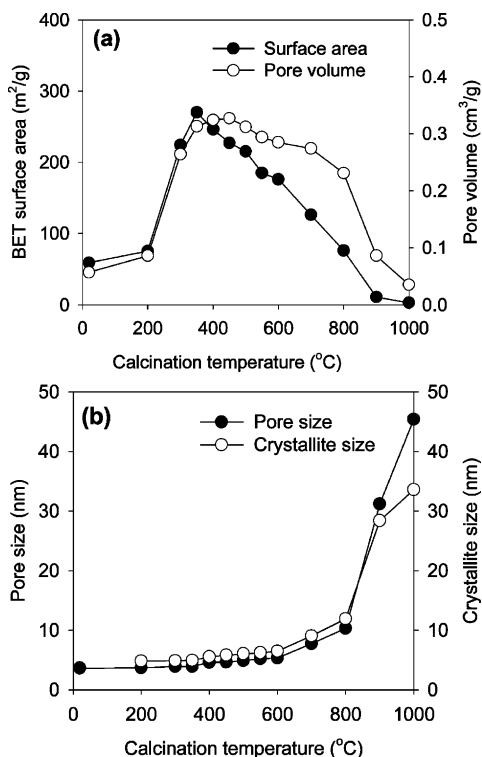
**Figure 11.** Structural evolution of TiO$_2$ (S$_{PF6,T80}$) prepared via [bmim]-[PF$_6$]- and surfactant-assisted sol−gel method upon heat treatment: (a) surface area and pore volume and (b) average pore size and crystallite size.

tion Figure S4). For S$_{PF6,T80}$ from as-synthesized to calcined up to 900 °C, only anatase peaks existed, and the crystallite size increased from ∼5 to ∼28 nm. The corresponding evolution of their structural properties is summarized in Table 2 and Figure 11. In this surfactant-templated methods, where organic residues in the TiO$_2$ sol−gel network are removed during heat treatment, the surface area and pore volume of S$_{PF6,T80}$ increased to a large extent, reached to a plateau at 350 °C, and then decrease significantly due to concurrent effect of template removal and pore collapse as increasing heat-treatment temperature. Comparing TiO$_2$ particles calcined at high temperatures (e.g., 500 °C) due to their high crystallinity and absence of impurities, which are important factors for achieving enhanced photocatalytic activity, S$_{PF6,T80}$ had high surface area of above 200 m$^2$/g and porosity of 50%. Moreover, with increasing calcination temperature from 350 °C to 600 °C, the pore size was controllable from ∼3.6 to ∼5.3 nm without significant reduction of pore volume.

**Photocatalytic Activity.** The photocatalytic activity of S$_{PF6,T80}$ calcined at 500 °C was evaluated in comparison with S$_{PF6}$ and P-25 TiO$_2$ (Degussa), one of the most promising and widely used photocatalysts. The results shown in Figure 12 revealed that the photocatalytic activity of S$_{PF6,T80}$ was significantly improved as compared to that of S$_{PF6}$. Further-more, S$_{PF6,T80}$ had almost similar or slightly less photocata-lytic activity to P-25. Considering the versatile application of the sol−gel method used in this study, which enables TiO$_2$ material to be shaped in form of powders, films, and membranes, S$_{PF6,T80}$ is comparable to P-25, which is con-sidered a nonporous material prepared via flame hydrolysis of TiCl$_4$ for making powders.[2,46] Furthermore, compared with P-25, which is generally composed of well-dispersed nano-particles with a size of around 30 nm, S$_{PF6,T80}$ consists of
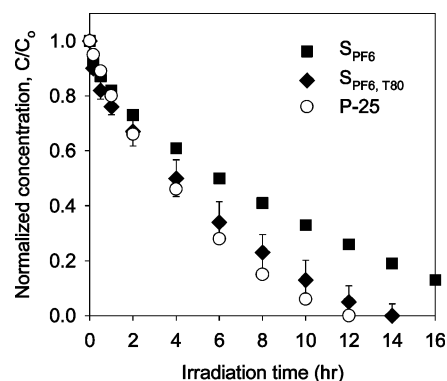


**Figure 12.** Photocatalytic degradation of 4-chlorophenol by commercially available TiO$_2$ (P-25), [bmim][PF$_6$]-templated TiO$_2$ (S$_{PF6}$), and [bmim][PF$_6$]- and surfactant-templated TiO$_2$ (S$_{PF6, T80}$).

tiny primary particles (less than 5 to 20 nm, depending on calcination temperature) agglomerated into big clusters (larger than 200 nm as shown in Supporting Information Figure S2). The big clusters could be advantageous in certain applications utilizing catalysts in suspension because they are easier to recover.

## Conclusions

In this study, nanostructured TiO$_2$ particles with high surface area, controlled porosity, and narrow pore size distribution have been synthesized via a sol−gel method modified with RTILs and surfactant molecules. Due to the special characteristics of the [bmim][PF$_6$] as well as the role of surfactant as a pore templating material in sol−gel network, highly porous TiO$_2$ particles with anatase crystalline structure were formed even at low temperatures. The TiO$_2$ particles were thermally stable and thus resistant to pore collapse and anatase-to-rutile phase transformation during calcination. The thermal stability induced high photocatalytic activity after heat treatment of TiO$_2$ particles up to 800 °C, and the activity was comparable to that of Degussa P-25 TiO$_2$. This synthesis method has important implications since obtaining crystal structure at low temperatures and keeping good photocatalytic activity at high temperatures can make it possible to utilize the TiO$_2$ particles and their preparative method in various applications. This new methodology using ionic liquid and surfactant in combination can also be useful for preparing similar crystal nanostructures of other oxide materials at low temperatures.

**Supporting Information Available:** HR-TEM images of S$_{BF4}$ (Figure S1); particle size of as-synthesized and calcined S$_{control}$, S$_{PF6}$, and S$_{BF4}$ (Figure S2); size measurement of Tween 80 surfactant self-assembly (Figure S3); and XRD patterns of S$_{PF6,T80}$ upon heat treatment (Figure S4). This material is available free of charge via the Internet at http://pubs.acs.org.

(46) Ettlinger, M. Technical Bulletin Pigments, No. 56, Degussa AG.